Journal of Inorganic Biochemistry 104 (2010) 820–830

Contents lists available at ScienceDirect

Journal of Inorganic Biochemistry

journal homepage: www.elsevier.com/locate/jinorgbio

Synthesis, structural and spectroscopic characterization and biomimetic properties of new copper, manganese, zinc complexes: Identification of possible superoxide-dismutase mimics bearing hydroxyl radical generating/scavenging abilities

Giulio Lupidi [a], Fabio Marchetti [b], Norberto Masciocchi [c], Daniel L. Reger [d], Sartaj Tabassum [e], Paola Astolfi [f], Elisabetta Damiani [g], Claudio Pettinari [b,*]

[a] Dipartimento di Biologia Molecolare Cellulare e Animale, Università degli Studi di Camerino, Via Madonna delle carceri, I-62032 Camerino, MC, Italy
[b] Dipartimento di Scienze Chimiche, Università degli Studi di Camerino, Via S. Agostino 1, I-62032 Camerino, MC, Italy
[c] Dipartimento di Scienze Chimiche e Ambientali, Università dell'Insubria, Via Valleggio 11- 22100 Como, Italy
[d] Department of Chemistry and Biochemistry, University of South Carolina, Columbia, SC, 29208, USA
[e] Department of Chemistry, Aligarh Muslim University, Aligarh, 202002, India
[f] Dipartimento ISAC-Sezione Chimica, Università Politecnica delle Marche, I-60131 Ancona, Italy
[g] Dipartimento di Biochimica, Biologia e Genetica, Università Politecnica delle Marche, I-60131 Ancona, Italy

ARTICLE INFO

Article history:
Received 20 January 2010
Received in revised form 22 March 2010
Accepted 23 March 2010
Available online 7 April 2010

ABSTRACT

A series of Cu(II), Zn(II) and Mn(II) coordination compounds has been synthesized by reaction of the corresponding metal salts and pyrazolyl-based ligands, i.e. the neutral 1-(2-(4-((2,2,2-tri(1H-pyrazol-1-yl)ethoxy)methyl)benzyloxy)-1,1-di(1H-pyrazol-1-yl)ethyl)-1H-pyrazole {*p*-$C_6H_4[CH_2OCH_2C(pz)_3]_2$, ($L^1$), and the anionic hydridotris(3-phenyl-5-methylpyrazolyl)borate $(L^2)^-$, bis(pyrazolyl)acetate (L^3) and bis(3,5-dimethylpyrazolyl)acetate $(L^4)^-$: the species $[L^1(CuCl_2)_2]$ (**1**), $[L^1(Cu(OAc)_2)_2]$ (**2**), $[L^1(Zn(OAc)_2)_2]$ (**3**), $[(CuCl(L^2)(Hpz^{Ph,Me})]$ (**4**), $[Mn(L^3)_2]\cdot 2H_2O$, (**5**), $[ZnCl(L^3)(imH)]\cdot MeOH$ $[CuCl(L^4)(imH)]\cdot 2H_2O$ (**7**) have been obtained ($Hpz^{Ph,Me}$ = 3-phenyl-5-methylpyrazole, imH = imidazole). Complexes **1** and **4** have been structurally characterized, also using less conventional powder diffraction methods. The superoxide scavenging activity has been characterized by indirect assays including EPR analysis. All complexes exhibit superoxide scavenging activity with IC_{50} in the μM range and they protect against the oxidative action of peroxynitrite in different ways. **1**, **4** and **7** exert both an anti- and pro-oxidant effect depending on their concentration as evaluated by EPR and fluorescence methods. The pro-oxidative effects are absent in Zn(II) and Mn(II) complexes.

1. Introduction

The formation of reactive oxygen species (ROS) and the well known deleterious consequences of their uncontrolled production, is the price that respiring organisms have to pay during their life cycle. Hence, all aerobic organisms have developed a host of defence mechanisms aimed at minimizing, either directly or indirectly, the formation or propagation of ROS. For example, one such line of defence is constituted by antioxidant enzymes, such as the superoxide dismutases (SOD) which catalytically scavenge the superoxide radical, an important agent of oxygen toxicity [1,2]. However, under certain circumstances, the imbalance between oxygen toxicity and antioxidant levels may call forth the need for exogenously administered compounds, either naturally occurring or completely synthetic molecules, which could augment endogenous cellular defence levels. In this context, the failure of clinical attempts to use SOD, due to several reasons (instability, immunogenicity, bio-inaccessibility, high molecular weight) has lead to the development of a number of low molecular weight SOD mimics which could ideally overcome these limitations. These compounds all bear a redox active metal centre, similar to the active site metals of the native SODs, i.e. Cu, Fe, Zn or Mn complexes with ligands of different chemical nature, capable of detoxifying superoxide radical [3–5]. Studies on the reactivity of low molecular weight complexes which exhibit SOD like activity have attracted major attention for the development of SOD mimics and for expanding the biomimetic chemistry of transition metals complexes. The pharmaceutical use of metal complexes has therefore excellent potential and a broad array of medicinal applications have been investigated as summarized by several recent reviews in this field [6–9]. Different problems should be addressed during the use of SOD-mimics such as accumulation, biodistribution and clearance of metal ions bound to the complex. For this purpose it is necessary to consider the physiological responses of

* Corresponding author. Fax: +39 0737637345.
E-mail address: claudio.pettinari@unicam.it (C. Pettinari).

0162-0134/$ – see front matter © 2010 Elsevier Inc. All rights reserved.
doi:10.1016/j.jinorgbio.2010.03.013

these candidate drugs with *in vitro* and *in vivo* studies before they enter clinical trials. For the potential therapeutic use of metals in medicine, several efforts have been made to obtain compounds with high catalytic activity and different ligands have been used to increase their stability under physiological conditions [6,8,10]. Important requirements for SOD-like activity of the complexes appear to be a medium strength donor power, flexibility of the ligands and coordination sites belonging to N-heteroaromatic rings. Among the most successful metal-complexes possessing SOD activity, dinuclear metal complexes [11,12] have received much attention considering that in nature various enzymes containing dinuclear metal active centres exist and are able to bind oxygen and catalyze the transformation of reactive intermediates. As part of this ongoing search for new therapeutic antioxidant agents, we have decided to start a systematic study on copper, zinc and manganese complexes containing heterocyclic N-donor ligands, also able to form dinuclear species, followed by investigations on their superoxide scavenging activity [13–16].

Here we report on the synthesis of novel mono-, di and polynuclear metal complexes based on different types of ligands (Scheme 1), i.e. the neutral ligand 1-(2-(4-((2,2,2-tri(1H-pyrazol-1-yl)ethoxy)methyl)benzyloxy)-1,1-di(1H-pyrazol-1-yl)ethyl)-1H-pyrazole (L^1), and the anionic ligands hydridotris(3-phenyl-5-methylpyrazolyl)borate $(L^2)^-$, bis(pyrazolyl)acetate $(L^3)^-$ and bis(3,5-dimethylpyrazolyl)acetate $(L^4)^-$ bearing either Cu(II) [17], Zn(II) [18], Mn(II) [19], as active metal centres. Several zinc [20–23], copper [24–29] and manganese derivatives [30–32] have already been reported with ligands $(L^2)^-$, $(L^3)^-$ and $(L^4)^-$ [33,34]. The structural, spectroscopic and biochemical properties of the obtained metal complexes will be presented, including evaluation of SOD-like activity, effects on H_2O_2 decomposition/peroxidase activity and on peroxynitrite.

2. Experimental section

2.1. Materials and methods

Hypoxanthine (HX), xanthine, xanthine oxidase (XO, from bovine milk), superoxide dismutase (SOD, from bovine erythrocytes), catalase (CAT, from bovine liver) cytocrome c, phenazine methosulfate (PMS), β-nicotinamide adenine dinucleotide (NADH), nitroblue-di tetrazolium chloride (NBT) were obtained from Sigma Chemical Co. (Milan, Italy) while all other chemicals and reagents including the spin trap 5,5-dimethyl-1-pyrroline-N-oxide (DMPO) were purchased from Aldrich Chemical Co. (Milan, ITALY). DMPO was used as purchased since it gave no EPR signals when scanned at 100 mM concentration. Xanthine was dissolved in 1 μM NaOH. All compounds tested were dissolved in DMSO. Peroxynitrite was synthesized according to the protocol reported by Uppu et al. [35] and stored at −80 °C.

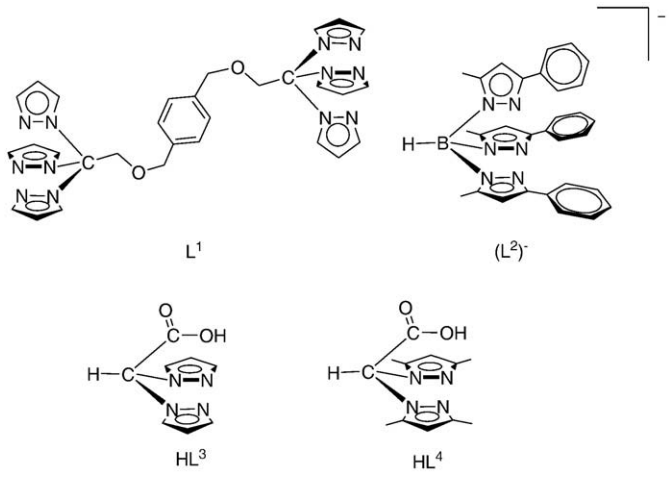

Scheme 1.

All the reactions and manipulations were performed in air. Solvent evaporations were always carried out under vacuum using a rotary evaporator. The samples for microanalysis were dried *in vacuo* to constant weight (20 ° C, ca.0.1 Torr). Elemental analyses (C, H, N) were performed in-house with a Fison Instrument 1108 CHNS-O Elemental analyzer. IR spectra were recorded from 4000 to 200 cm^{-1} with a Perkin-Elmer Spectrum 100 FT-IR instrument. The intensity of reported IR signals is defined as w = weak, m = medium and s = strong. ^1H and $^{13}C\{^1H\}$ NMR spectra were recorded on a 400 Mercury Plus instrument operating at room temperature (400 MHz for ^1H, 100 MHz for ^{13}C). H and C chemical shifts (δ) are reported in parts per million (ppm) from $SiMe_4$ (^1H and ^{13}C calibration by internal deuterium solvent lock). Peak multiplicities are abbreviated: singlet, s; doublet, d; triplet, t; quartet, q; multiplet, m. Melting points are uncorrected and were taken on an STMP3 Stuart scientific instrument and on a capillary apparatus. The electrical conductivity measurements (Λ_M, reported as $\Omega^{-1}\,cm^2\,mol^{-1}$) of acetonitrile and water solutions of the complexes were taken with a Crison CDTM 522 conductimeter at room temperature. Electrospray mass spectra were obtained with a Series 1100 MSI detector HP spectrometer, using MeOH as mobile phase. Solutions for electrospray ionization mass spectrometry (ESI-MS) were prepared using reagent grade methanol and/or acetonitrile and obtained data (masses and intensities) were compared to those calculated by using the IsoPro isotopic abundance simulator [36]. Peaks containing copper(II) and zinc ions are identified as the centres of isotopic clusters. The magnetic susceptibilities were measured at room temperature (22 °C) by the Gouy method, with a Sherwood Scientific Magnetic Balance MSB-Auto, using $HgCo(NCS)_4$ as calibrant and corrected for diamagnetism with the appropriate Pascal constants. The magnetic moments (in BM) were calculated from the equation $\mu_{eff} = 2.828\,(\chi_m^{corr}\,T)^{1/2}$. UV–visible (UV/Vis) Spectra were recorded on a Shimadzu — 1700 UV–Vis spectrometer and the data are reported as λ_{max}/nm. Cyclic voltammetric studies were performed on a CH Instrument Electrochemical Analyzer in a single compartmental cell with 0.4 M KNO_3 as supporting electrolyte. A three electrode configuration was used comprising of a Pt wire as auxiliary electrode, platinum micro cylinder as working electrode and Ag/AgCl as the reference electrode. Electrochemical measurements were made under a dinitrogen atmosphere. All electrochemical data were collected at 298 K and are uncorrected for junctions potentials. The formal potentials, E° (or voltammetric $E_{1/2}$) were taken as the average of the anodic (E_{pa}) and cathodic peak potentials (E_{pc}) obtained from the cyclic voltammetry.

2.2. Synthesis and characterisation of the ligands

2.2.1. 1-(2-(4-((2,2,2-Tris(pyrazol-1-yl)ethoxy)methyl)benzyloxy)-1, 1-di(pyrazol-1-yl)ethyl)-pyrazole (L^1)

The ligand L^1 was prepared by a slight modification of a previously reported synthesis [37]. α,α'-Dibromo-p-xylene, p-$(BrCH_2)_2C_6H_4$ (2.64 g, 10 mmol) and tris-2,2,2-(1-pyrazolyl)ethanol, $HOCH_2C(pz)_3$ (4.88 g, 20 mmol) were dissolved in dry tetrahydrofuran (THF) (125 ml). This solution was added drop wise to a suspension of NaH (1.5 g) in dry THF (300 ml) under an inert atmosphere. The mixture was stirred under reflux for 48 h and then allowed to cool at room temperature. To this solution, water (200 ml) was added drop wise to consume the excess NaH and dissolve the resulting NaBr and NaOH. The THF mixture was extracted with diethyl ether (4 × 100 ml) and the combined organic extracts were washed with 100 ml saturated $NaHCO_3$ solution with 100 ml NaCl solution and finally with 100 ml water. The organic layer was dried over anhydrous Na_2SO_4, filtered and the solvent removed under vacuum to afford the desired compound as a white–yellow powder (8.4 mmol, 4.95 g, 84%). M.p. 150–155 °C. Anal. calcd

for $C_{30}H_{30}N_{12}O_2$. C, 60.96; H, 5.07; N, 28.45. Found: C, 61.07; H, 4.98, N, 28.70. IR (nujol, mull, cm^{-1}): 3148w, 3133w, 3104w, 2944w, 2891w, 1516 m. ^1H NMR ($CDCl_3$): δ, 7.65, 7.38 (d,m, 3H, 3H, $J = 1.6$ Hz, 3,5-H pz), 7.18 (m,2H, C_6H_4), 6.32 (d of d, 3H, $J_{HH} = 2.5$, 4-H pz), 5.07 (s, 2H, OCH_2Ph), 4.44 (s, 2H, OCH_2 $(pz)_3$).

2.2.2. Potassium hydridotris(3-phenyl-5-methylpyrazolyl)borate: K[L²]

The potassium salt of the ligand hydridotris(3-phenyl-5-methylpyrazolyl)borate was synthesized according to the literature [38].

2.2.3. Bis(pyrazol-1-yl)acetic acid (HL³) and bis(3,5-dimethylpyrazol-1-yl) acetic acid (HL⁴)

The ligands HL^3 (HL^3 = bis(pyrazol-1-yl)acetic acid) and HL^4 (HL^4 = bis(3,5-dimethylpyrazol-1-yl)acetic acid) were prepared according to literature methods. Their analytical and spectroscopic data correspond to those reported in the literature [39,40].

2.3. Syntheses and characterization of the complexes

2.3.1. {(L¹)[CuCl₂]₂}, **1**

To a stirred solution of L^1 (0.59 g, 1.0 mmol) in dichloromethane, $CuCl_2 \cdot 2H_2O$ (0.342 g, 2.0 mmol), dissolved in methanol, was added. The reaction mixture was heated at reflux for 6 h, then concentrated to half of its volume by rotary evaporation, and kept for 3 days at 4 °C. A microcrystalline compound was obtained which was washed with methanol and shown to be compound **1**. The compound is soluble in DMSO. M.p 214 °C. Elem. Anal. Calcd. For $C_{30}H_{30}Cl_4Cu_2N_{12}O_2$:C, 41.92; H, 3.52; N, 19.55. Found: C, 41.76; H, 3.43; N, 19.23%. Λ_m (DMSO, 10^{-4} M, 293 K): 38.7 Ω^{-1} cm^2 mol^{-1}. $\mu_{eff} = 2.20$ BM. IR (nujol, mull, cm^{-1}): 3179w, 3142w, 3074w (C–H) 1586w, 1511w, 615 m, 603 m, 498w, 476w, 409 m, 401 m, 386w, 295 s (Cu–Cl).

2.3.2. {(L¹)[Cu(OAc)₂]₂}, **2**

To a stirred solution of L^1 (0.59 g, 1.0 mmol) in dichloromethane, $Cu(OAc)_2 \cdot 2H_2O$ (0.434 g, 2.0 mmol) dissolved in methanol was added. The reaction mixture was heated at reflux for 6 h, then evaporated and the residue washed with a dichloromethane/diethyl ether mixture. A micro-crystalline compound was obtained which was washed with methanol and shown to be compound **2**. The compound is soluble in DMSO and MeCN. M.p 160–165 °C. Elem. Anal. Calcd. For $C_{38}H_{42}Cu_2N_{12}O_{10}$: C, 47.85; H, 4.44; N, 17.62. Found: C, 47.45; H, 4.54; N, 17.93%. Λ_m (MeCN, 10^{-4} M, 293 K): 3.0 Ω^{-1} cm^2 mol^{-1}. $\mu_{eff} = 1.87$ BM. IR (nujol, mull, cm^{-1}): 3131w, 2935w (C–H) 1562 s, 1517 m, 1420 s.

2.3.3. {(L¹)[Zn(OAc)₂]₂}, **3**

Compound **3** was synthesized following a procedure analogous to that reported for **2**. To a stirred solution of L^1 (0.59 g, 1.0 mmol) in dichloromethane, $Zn(OAc)_2 \cdot 2H_2O$ (0.44 g, 2.0 mmol) dissolved in methanol (5 mL) was added. The solution was stirred overnight, then evaporated to half of its volume and refrigerated at 4 °C until a colorless precipitate formed, which was filtered, washed with diethyl ether and shown to be compound **3**. The compound in insoluble in all organic solvents. M.p 204 °C. Elem. Anal. Calcd. For $C_{38}H_{42}N_{12}O_{10}Zn_2$: C, 47.66; H, 4.42; N, 17.55. Found: C, 48.11; H, 4.62; N, 18.11%. IR (nujol mull, cm^{-1}): 1664 s, 1583br, 1516 m, 1473w, 1446 m(C=O), 437 m, 426 m.

2.3.4. [(CuCl(L²)(Hpz^Ph,Me)], **4**

To a stirred solution of K[L^2] (0.48 g, 1.0 mmol) in dichloromethane, $CuCl_2 \cdot 2H_2O$ (0.171 g, 1.0 mmol) was added. The reaction mixture was stirred at room temperature for 6 h, then filtered off and the solution evaporated. A pale-green residue formed which was washed with diethyl ether and shown to be compound **4**. The compound is soluble in chlorinated solvents and DMSO. Re-crystallised from dichloromethane/diethyl ether. M.p 170 °C. Elem. Anal. Calcd. for $C_{40}H_{38}BClCuN_8$: C, 64.87; H, 5.17; N, 15.13. Found: C, 64.35; H, 5.36; N, 14.75%. Λ_m (MeCN, 10^{-4} M, 293 K): 22.3 Ω^{-1} cm^2 mol^{-1}. ESI MS (CH_3CN) (+): 704 $[(Cu(L^2)(Hpz^{Ph,Me})]^+$. $\mu_{eff} = 1.81$ BM. IR (nujol mull, cm^{-1}): 3215 (NH), 2526m (BH), 1565w, 1540m, 1503m, 524m, 495m, 478w, 438w, 388w, 318w, 304w, 280br (Cu–Cl).

2.3.5. [(Mn(L³)₂]·2H₂O, **5**

To a stirred solution of HL^3 (0.193 g, 1.0 mmol) in methanol, a methanol solution of $MnCl_2 \cdot 6H_2O$ was added (0.234 g, 1.0 mmol). The reaction mixture was stirred for 6 h. An amorphous colorless powder was obtained, washed with methanol and n-hexane and shown to be compound **5**. The compound is soluble in DMSO. Re-crystallised from MeOH. M.p. 230 °C. Elem. Anal. Calcd. for $C_{16}H_{18}MnN_8O_6$, C, 40.60; H, 3.83; N, 23.67; O, 20.28. Found: C, 40.40; H, 3.76; N, 23.23; O, 19.80%. Λ_m (MeCN, 10^{-4} M, 293 K): 2.5 Ω^{-1} cm^2 mol^{-1}. $\mu_{eff} = 5.96$ BM. IR (nujol, cm^{-1}): 3360br, 3114w (CH), 1657m, 1626m, 1528m, 1513m, 1455m (C=O), 417m, 229w.

2.3.6. [(Zn(OAc)(L³)(Him)]·MeOH, **6**

To a stirred solution of HL^3 (1 mmol, 0.248 g) in methanol, Zn $(OAc)_2 \cdot H_2O$ (2.0 mmol)) and imidazole (2.0 mmol), were added. The reaction mixture was stirred for 6 h. A light colorless amorphous powder was obtained, which was washed with methanol and shown to be compound **6**. The compound is soluble in DMSO. M.p. 132–135 °C. Elem. Anal. Calcd. For $C_{18}H_{26}N_6O_5Zn$: C, 45.82; H, 5.55; N, 17.81. Found: C, 46.00; H, 5.85; N, 17.62%. Λ_m (MeCN, 10^{-4} M, 293 K): 3.2 Ω^{-1} cm^2 mol^{-1}. IR (nujol mull, cm^{-1}): 3128w (CH), 1631s, 1513m, 1441m (C=O) 402w.

2.3.7. [(CuCl(L⁴)(Him)]₂·2H₂O, **7**

To a stirred solution of HL^3 (1 mmol, 0.248 g) in methanol, $CuCl_2 \cdot H_2O$ (2.0 mmol) and imidazole (2.0 mmol), were added. The reaction mixture was stirred for 6 h. A light blue amorphous powder was obtained, which was washed with methanol and shown to be compound **7**. The compound is soluble in DMSO. M.p. 217–220 °C. Elem. Anal. Calcd. For $C_{30}H_{42}Cl_2Cu_2N_{12}O_6$: C, 41.67; H, 4.90; N, 19.44. Λ_m (MeCN, 10^{-4} M, 293 K): 3.5 Ω^{-1} cm^2 mol^{-1}. Found: C, 42.00; H, 4.75; N, 19.71%. $\mu_{eff} = 1.52$ BM. IR (nujol mull, cm^{-1}): 3200br, 3158w, 3128w (CH) 1662 s, 1640sh, 1557 m, 1534w, 1500w, 1446 (C=O), 430w, 417w, 226 m. ESI MS (CH_3CN) (+): 657 $[Cu_2Cl(L^4)_2]^+$.

2.4. Crystal structures determination

2.4.1. Single-crystal X-ray structure determination of [(CuCl(L²)(Hpz^Ph,Me)], **4**

A crystal of [(CuCl(L^2)($Hpz^{Ph,Me}$)] with approximate dimensions 0.12 × 0.20 × 0.25 mm was mounted on the tip of a glass fiber and put on a goniometer head. Diffraction measurements were performed on an Enraf-Nonius CAD4 diffractometer using graphite monochromated Mo-Kα radiation. Data collection (ω-scans) and processing (cell refinement, data reduction and empirical absorption correction) were performed using the locally available programs. The structure was solved by direct methods using SHELXS-97 [41] and refined by full-matrix least-squares techniques on F^2 with SHELXL-97. All hydrogen atoms were located by difference maps and were refined isotropically as riding on their pertinent C, or N atoms. Table 1 contains a summary of crystal data, data collection parameters and structural analysis. Crystallographic data for the structural analysis (including that reported below from powder diffraction data) have been deposited with the Cambridge Crystallographic Data Centre, CCDC No. 761615-761616. Copies of this information may be obtained free of charge on application to CCDC, 12 Union Road, Cambridge CB2 1EZ, UK (fax: 44 1223 336 033; e-mail: deposit@ccdc.cam.ac.uk or www: http://www.ccdc.cam.ac.uk).

2.4.2. Powder X-ray structure determination of {(L¹)[CuCl₂]₂}, **1**

A powdered, microcrystalline sample of **1** was gently ground in an agate mortar, then deposited in the hollow of an aluminium sample

Table 1
Summary of crystal data and refinement parameters for compounds **1** and **4**.

Compound	**1**	**4**
Formula	$C_{30}H_{30}Cl_4Cu_2N_{12}O_2$	$C_{40}H_{38}BClCuN_8$
Molecular weight (g mol^{-1})	859.56	740.58
Temperature (K)	293	293
Crystal system	Monoclinic	Triclinic
Space group	C2/c	P-1
Method	Powder	Single Crystal
Cell parameters	a = 13.5231(4) Å	a = 11.748(2) Å
	b = 11.6834(4) Å	b = 12.326(2) Å
	c = 22.8433(8) Å	c = 15.286(3) Å
	α = 90°	α = 102.07(2)°
	β = 109.997(2) °	β = 97.55(1)°
	γ = 90°	γ = 116.20(2)°
V (Å^3)	3391.6(2)	1870.0(6)
μM (cm^{-1})	48.82	6.93
Z	4	2
ρ_{calc} (g cm^{-3})	1.683	1.310
F(000)	1744	770
Radiation	Cu–Kα	Mo–Kα
2θ min–max	7.0–105.0	6.0–50.6
Independent refl. (or *y* data)/parameters	4901/50	6805 / 468
R(int)	n.a.	0.070
R_p, R_{wp}, R_{Bragg}	0.026. 0.040, 0.024	n.a
R, wR_2	n.a	0.0529, 0.0979

holder (equipped with a zero-background plate). Diffraction data were collected with overnight scans (16 h long) in the 5–105° 2θ range on a Bruker AXS D8 Advance diffractometer, equipped with a linear position-sensitive Lynxeye detector, primary beam Soller slits, and Ni-filtered Cu–Kα radiation (λ = 1.5418 Å); sampling interval (in continuous mode): Δ2θ = 0,02°. divergence slit: 1.0°; goniometer radius 300 mm; generator setting: 40 kV, 40 mA. Standard peak search, followed by indexing with TOPAS [42] allowed the detection of the approximate unit cell parameters later improved by LeBail refinements. Indexing figure of merit M(22) = 61.5. Space group determination, performed using systematic extinction conditions, in conventional mode as well using a structureless full pattern profile match, indicated *C2/c* as probable space group (later confirmed by successful structure solution and refinement). Structure solution was performed (by the simulated annealing technique) as implemented in TOPAS, using for "half" organic ligand (the crystallographic independent portion) a rigid, idealized model [43], (flexible at the C-pyrazole links and at the saturated O and C chain atoms) and one independent metal and two chloride ions. The final refinements were carried out by the Rietveld method, maintaining the rigid bodies described above (with the organic ligands bisected by a twofold axis). Peak shapes were defined by the Fundamental Parameters Approach implemented in TOPAS, while crystal size effect was modelled by a Lorentzian broadening. The background contribution to the total scattering was modelled by Chebyshev's polynomials, also accounting for a structured trace below Bragg peaks. One, refinable isotropic thermal parameter was assigned to the metal atom, augmented by 2.0 Å^2 for lighter atoms. No preferred orientation correction was found to be necessary. The final Rietveld refinement plot is shown in Fig. 1. Table 1 contains a summary of crystal data, data collection parameters and structural analysis.

2.5. In vitro evaluation of radical scavenging activity

2.5.1. Evaluation of superoxide radical scavenging activity

Superoxide dismutase (SOD) activity of the complexes was determined with a nonenzymatic assay method. Superoxide radicals were generated by the NADH/PMS system according to ref. [44]. The mixture (1 ml) in 20 mM potassium phosphate buffer contained NBT 43 μM, NADH 166 μM, aliquots of compounds in DMSO (from 0 to 30 μM), and PMS 2.7 μM that was added to start the reaction. The reaction was conducted at room temperature for 2 min. The reduction of NBT to the blue chromogen formazan by superoxide radical was monitored at 560 nm.

2.5.2. Hydroxyl radical assay

The deoxyribose method for determining the scavenging effect of the SOD mimics on hydroxyl radicals was performed according to the method previously described in [45].

2.5.3. EPR spin trapping of superoxide radical with DMPO

Samples were assayed by EPR spectrometry for superoxide radical dismutation activity using XO (0.4 u/ml) mediated oxidation of HX (1 mM) as a source of superoxide and employing DMPO (100 mM) as spin trap. Experiments were carried out in PBS (100 mM phosphate buffer, pH 7.4, 0.9% NaCl), 1 mM DTPA in a final volume of 150 μl. Test compounds were prepared in DMSO and used at several concentrations (max. conc of DMSO used was 10% v/v). As a control, the test compound was replaced by DMSO (10% v/v). The reaction was started by addition of XO, and after thorough mixing, the mixture was transferred to a Pasteur pipette whose narrow end was sealed off using a Bunsen burner flame which served as sample cell, and the EPR spectra recorded 90 s after XO addition. EPR spectra were collected on a Bruker EMX EPR spectrometer (Bruker, Karlsruhe, Germany) equipped with an XL Microwave frequency counter with the following settings: frequency 9.78 GHz, power 25 mW, modulation amplitude 1 G, gain 5×10^5, field width 100 G, time constant 1.28 ms and scan time 42 s. For each experiment, 10 scans were recorded.

2.5.4. EPR spin trapping of hydroxyl radical with DMPO

Hydroxyl radical generating ability from test compounds was examined by their addition to a reaction mixture containing 1 mM H_2O_2 in the presence of 100 mM DMPO in PBS, 1 mM DTPA in a final volume of 150 μl. The reaction was started by addition of H_2O_2 and after thorough mixing, the mixture was transferred to a sample cell and EPR spectra recorded 90 s after H_2O_2 addition as described above.

Hydroxyl radical scavenging ability of test compounds was examined by their addition to the hydroxyl radical-generating Fenton system consisting of 50 μM ferrous ammonium sulphate, 1 mM H_2O_2 in the presence of 100 mM DMPO in PBS, 1 mM DTPA in a final volume of 150 μl. The reaction was started by addition of H_2O_2 and after thorough mixing, the mixture was transferred to a sample cell and EPR spectra recorded 90 s after H_2O_2 addition as described above.

2.5.5. Evaluation of peroxidase activity

Peroxidase activity was monitored using the DCFH fluorescence method. This activity can be conveniently measured by monitoring

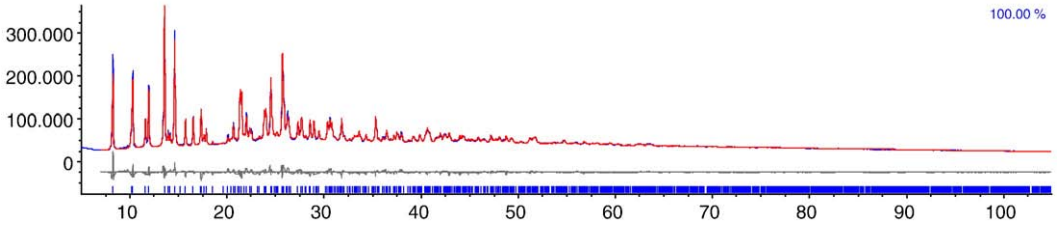

Fig. 1. Rietveld refinement plot for species **1**, with difference plot and peak markers at the bottom. Horizontal axis, 2θ, °; vertical axis, counts.

oxidation of dichlorodihydrofluoresceine diacetate hydrolyzed freshly for every experiment according to the published procedure [46]. Briefly, DCFH dissolved in ethanol was hydrolyzed by NaOH (0.01 M) in the dark for 30 min at room temperature and stored in an ice bath during the experiment. Peroxidase activity was measured as follows: SOD-mimics were mixed with a solution of DCFH (2.5 μM) in phosphate buffer (50 mM, pH 7.4, DTPA 0.1 mM). The reaction was initiated by adding H_2O_2 and the increase in fluorescence emission due to DCF formation was monitored at 520 nm for 30 min. (excitation λ = 495 nm).

2.5.6. Measure of $ONOO^-$ scavenging activity

Peroxynitrite ($ONOO^-$) scavenging ability of different complexes was measured by monitoring the inhibition of oxidation of non-fluorescent DCFH to the highly fluorescent DCF. DCFH was prepared as previously described. To measure the scavenging activity of peroxynitrite, $ONOO^-$ at a fixed concentration (0.02 mM) was added to DCFH (2.5 μM) in 2 ml of 50 mM phosphate buffer, pH 7.4, DTPA 0.1 mM, containing 25 μM of the different complexes, under continuous stirring and the solution was incubated at 25 °C for 15 min. After this time the fluorescence intensity of oxidized DCFH was measured at excitation and emission wavelengths of 490 and 520 nm respectively.

3. Results

3.1. Synthesis of ligands and complexes

The reaction between 1,4-$C_6H_4[CH_2OCH_2C(pz)_3]_2$ (L^1) and $CuX_2 \cdot nH_2O$ (X = Cl, or OAc) in a mixture of dichloromethane and methanol always yielded complexes of formula $[(L^1)(CuX_2)]$, (**1**: X = Cl, **2**: X = OAc) (Scheme 2) independent of the stoichiometric ligand to metal ratio employed, insoluble in MeCN and chlorinated solvents and moderately soluble in DMSO, in which **2** is not-electrolyte, in contrast to **1** which exhibits a conductivity value typical of 1:1 electrolyte [47], suggesting only partial dissociation in DMSO upon breaking of the polymeric structure. Whereas in **2**, both acetate counterions likely remain coordinated to copper also in solution, as indicated by the conductivity value found [47]. The IR spectra show all bands due to the neutral bis(tripodal) ligands and to the counter-ion, and in the case of **2** the existence of a bridging acetate [48]. The reaction between L^1 and $Zn(OAc)_2$ yielded the 1:1 adduct **3** also when the reaction was carried out in strong ligand excess (Scheme 2).

The synthesis of the polypyrazolylborate ligand $Tp^{Ph,Me}$, here described, is essentially the same as that used to prepare the parent ligands Tp* by heating sodium or potassium tetrahydridoborate with an excess of the $Hpz^{Ph,Me}$ [49]. Hydrogen gas is evolved during the reaction and its progress was measured. The copper(II) chloro complex **4** was obtained from the reaction of two equivalents of $K[Tp^{Ph,Me}]$ with one equivalent of the copper salt in methanol and in dichloromethane, respectively, at room temperature and in good yields (Scheme 3). The presence of the neutral $Hpz^{Ph,Me}$ coordinated to copper, is due to the hydrolysis of excess $Tp^{Ph,Me}$, a phenomenon already observed [50]. The Mn complex $[Mn(L^3)_2]\cdot 2H_2O$ **5** was obtained from the reaction of two equivalents of the ligands HL^3 in MeOH with one equivalent of the metal salt (Scheme 3). Deprotonation of HL^3 occurs also in the absence of base. Whereas from the reaction of equimolar quantity of HL^4 with Zn and Cu salts in the presence of excess imidazole, derivatives **6** and **7** formed (Scheme 3).

3.2. Spectroscopic characterization

Due to the limited solubility of compounds **1**–**3**, polynuclear structures (see also below Section 3.3) were hypothesized for all of them, in which the L^1 ligand bridges two metal centres. IR spectral analysis seems in accordance with the proposed structures. In fact, in the IR spectrum of **1** only a strong band due to Cu–Cl stretching mode was observed at 295 cm^{-1}, that is indicative of only one terminal chloride. In the IR spectra of **2** and **3** a number of strong bands were found in the range of 1400–1700 cm^{-1}, assignable to ν(COO) of acetates. Such an high number of bands cannot give a straightforward indication of the bonding mode of acetates, however one could tentatively hypothesize that they are bridged between two metal

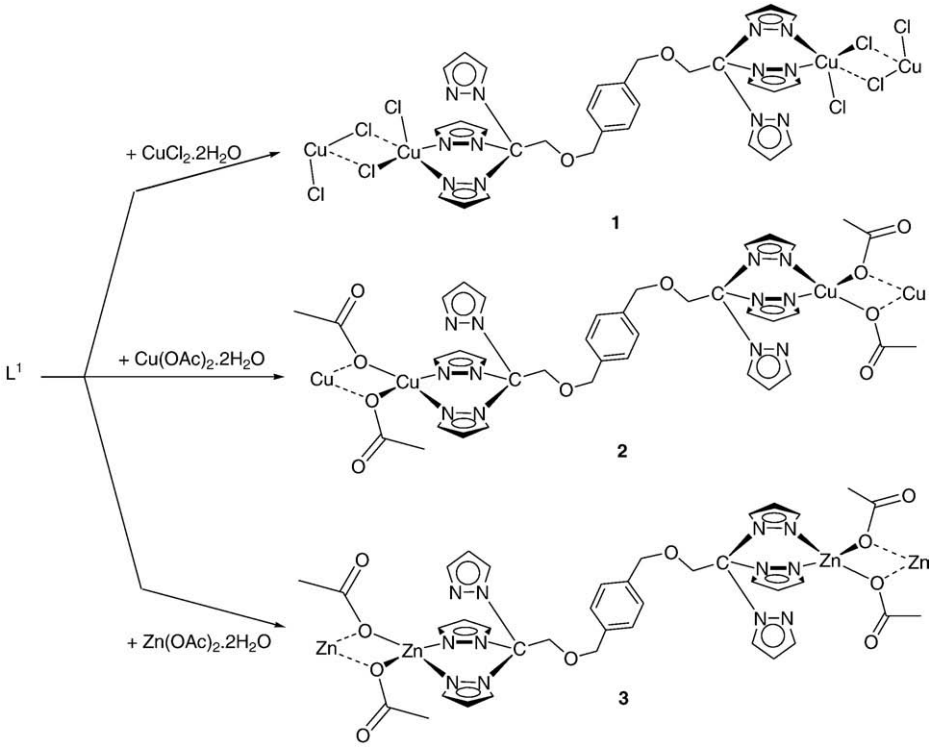

Scheme 2.

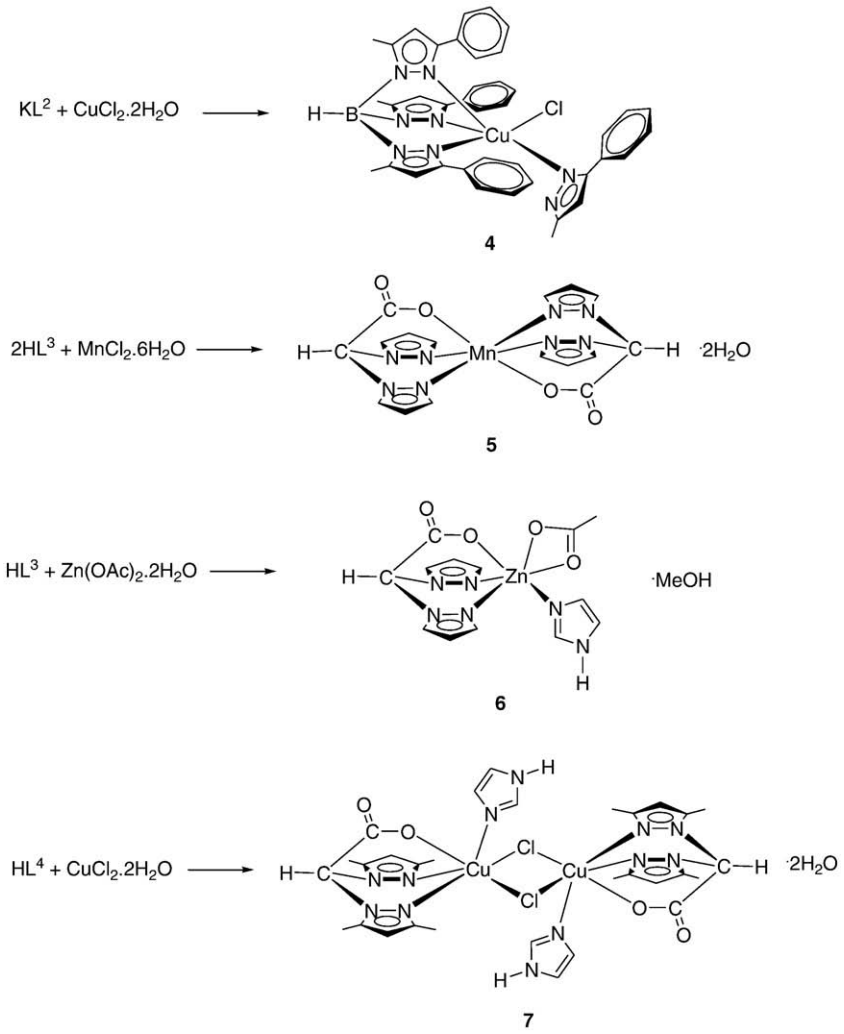

Scheme 3.

centres and also coordinated as terminal monodentates, as it is likely in the case of compound **3**, where a strong band was observed at 1664 cm^{-1}.

In the IR spectrum of compound **4** the typical ν(B–H) mode was found at 2526 cm^{-1}, together with an intense band at 3215 cm^{-1} due to the ν(N–H) of the 3-phenyl-5-methylpyrazole arising from decomposition of the $(L^2)^-$ ligand. Moreover a broad band at 280 cm^{-1} confirms the presence of a Cu–Cl bond. Finally, also the ESI-MS spectrum indicates the presence of a Cu environment containing the tris(pyrazol-1-yl) borate and the neutral pyrazole, as the peak at 704 can be easily attributed to the cationic fragment $[(Cu(L^2)(Hpz^{Ph,Me})]^+$.

The IR spectra of compounds **5**–**7** containing the bis(pyrazol-1-yl) acetate ligands, display the typical pattern due to monoanionic tridentate ligands, in which the carboxylate arm is also coordinated to the metal centre, the highest ν(COO) being always found in **5**–**7** at ca. 1630–1670 cm^{-1}, whereas uncoordinated carboxylate groups are generally observed at higher frequencies, above 1700 cm^{-1} [39,50].

The dinuclear nature of compound **7** was proposed mainly on the basis of the ESI-MS spectrum that shows a peak at 657 assignable to the cationic fragment $[Cu_2Cl(L^4)_2]^+$.

The magnetic measurements on the paramagnetic compounds **1**, **2**, **4**, **5** and **7** were performed to gain more information on the magnetic status of the metal centre: apart from the copper derivatives **1**, **2** and **4** that show dipole magnetic moments in the range of 1.87–2.20 B.M., typical of d^9 Cu(II) ions with a unique unpaired electron, the copper (II) derivative **7** displays a somewhat lower value of 1.52 B.M. which should indicate partial quenching of magnetism, due to super-exchange mechanisms through the bridging chloride ligands, whereas the manganese derivative **5** shows a value of 5.96 B.M., in accordance with a high spin d^5 Mn(II) centre, thus indicating that $(L^3)^-$ behaves as a weak-field ligand.

3.3. Structural characterization

$[L^1(CuCl_2)_2]$, **1**, is a polymeric complex, built upon Cu(II) dimers of $ClCu(\mu\text{-}Cl)_2CuCl$ formulation, connected in one-dimensional chains (shown in Fig. 2) by the large L^1 ligand.

Both the dimer and the ligand are located, in the crystal, onto a special position, an inversion centre for the former and a twofold axis for the latter. Since it is well known that powder diffraction methods on complex materials cannot attain the precision typical of conventional single-crystal structure determinations, a rigid body description (see Experimental section) was employed, in which only the flexible torsional freedom is tolerated. Accordingly, our model shows pentacoordinated Cu(II) ions in $CuCl_2N_2$ chromophores of square-pyramidal shape, in which the apical Cu–Cl distance (2.82) Å) is significantly longer than the equatorial ones (2.24–2.28 Å). Two nitrogen atoms, in *cis* position and *ca.* 2.08 Å apart from the metal centre complete the overall coordination, while the third pyrazolate residue is, surprisingly, non-coordinating, with a Cu···N distance of 3.21 Å. The presence of a vacant site on the Cu(II) ion and the odd conformation of what we (initially) thought being an ideal tripod-like

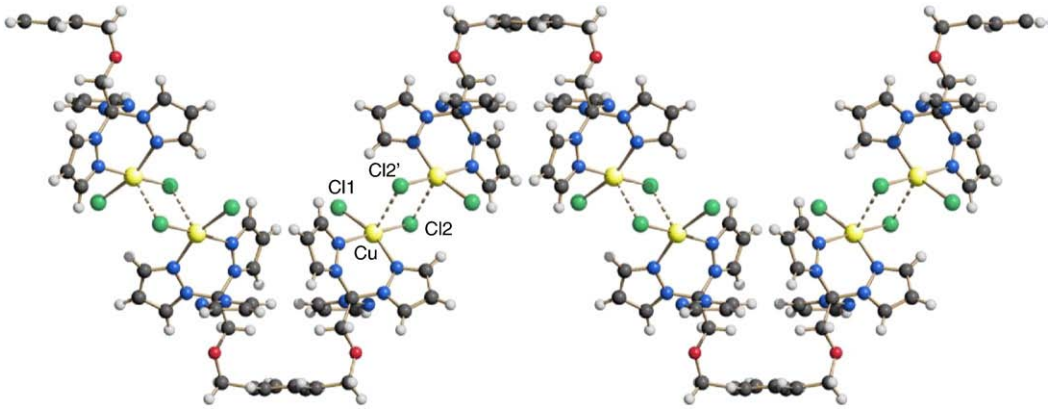

Fig. 2. Schematic drawing of: a portion of the polymeric species **1**, with partial labelling scheme. In the crystal, wavy chains run parallel to the [101] direction (the horizontal axis). Vertical axis, **b** (the twofold axes bisecting the external 1,4-substituted aromatic rings of the L^1 ligand). Relevant bond distances (Å) and angles (°): Cu–Cl1 2.278(9); Cu–Cl2 2.236(7), Cu–Cl2′ 2.818(9), Cu–N21 2.069(6), Cu–N31 2.084(6), Cl1–Cu–N31 162.8(3), Cl2–Cu–N21 176.8(4). Copper: yellow; Chlorine: green; Nitrogen: blue; Oxygen: red.

ligand, prompted us to verify which structure had to be considered correct, *i.e.* the open, or the closed one, or any intermediate conformation. Several tests performed using restrained torsional values (not shown here) clearly indicated that the open conformation is the correct one, as also witnessed by the very low profile and Bragg agreement factors.

Worthy of note, the overall crystal packing (not shown here) is generated by juxtaposition of infinite, parallel and wavy chains running along the [101] direction, with the L^1 ligand moieties alternating above, and below, the chain axis. This effect can be graphically appreciated in Fig. 2, where fragmented lines connect the longest Cu···Cl interactions.

At variance from **1**, species **4**, [(CuCl(L^2)($Hpz^{Ph,Me}$)], contains mononuclear Cu(II) complexes, the structure of which is schematically shown in Fig. 3; these molecules, in the crystal phase, weakly interact with neighbouring (symmetry equivalent) complexes through weak H···H (2.29–2.36 Å, and above) and H···Cl (2.90 Å) contacts.

Each Cu(II) centre is linked to a tripod-like L^2 ligand, to a monodentate 3-phenyl-5-methylpyrazole moiety and to a terminally bound chloride ion (Cu–Cl 2.2833(8) Å). The overall coordination geometry is close to trigonal–bipyramidal, with the apical positions

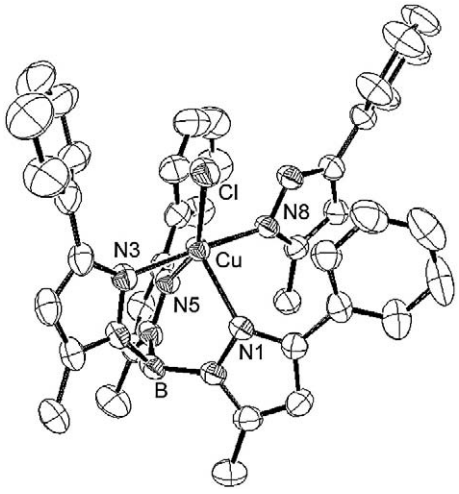

Fig. 3. ORTEP drawing of the species **4**, with partial labelling scheme. Thermal ellipsoids drawn at the 50% probability level. Hydrogen atoms omitted for clarity. Relevant bond distances (Å) and angles (°): Cu–Cl 2.2833(8), Cu N1 2.246(2), Cu N3 2.056(2), Cu N5 2.035(2), Cu N8 2.035(2). N1 Cu Cl 116.14(6), N3 Cu Cl 93.37(6), N5 Cu Cl 149.02(6), N8 Cu Cl 91.14(6), N3 Cu N1 89.43(8), N5 Cu N1 94.77(8), N8 Cu N1 88.78(8), N5 Cu N3 84.64(8), N8 Cu N3 175.49(8), N5 Cu N8 91.38(8).

defined by the Cu–N bond of the neutral ligand (2.034(2) Å), and of one pyrazolate branch of the tripodal moiety (2.056(2) Å). In such a crowded environment, phenyl rings of the tripod are (coherently, *i.e.* propeller-like) twisted at an angle (in the 30–40° range) with respect to the heteroaromatic rings. Similarly, also the torsional angle about the C13–C14 bond, linking the two aromatic rings in the 3-phenyl-5-methylpyrazole ligand, is significantly different from zero, approaching 38°. Under these structural conditions, the Cu(II) ions are deeply buried within the ligands sphere, but, thanks to a possible labilization of the Cu–N bond of the neutral moiety, ligand dissociation and substitution may occur, thus giving the whole complex a chemical reactivity which, *per se*, is not evident from the (rigid) solid-state structure.

3.4. Evaluation of superoxide radical scavenging activity

Different methods (non enzymatic and enzymatic methods) can be used to ascertain the Superoxide Radical Scavenging activity of various compounds. The SOD-like activity for the reaction of different mimics was determined studying the effect of the complexes on superoxide generated by the NADH/PMS system as described in materials and methods. This method is very sensitive for evaluation of superoxide radical scavenging activity and was used to calculate the IC_{50} of the most active compounds (Table 2). As reported, all complexes show a different rate of reaction with O_2^- radicals. Mimics [($Mn(L^3)_2$]·$2H_2O$ (**5**), [(CuCl(L^4)(Him)]$_2$·$2H_2O$ (**7**) and {(L^1)[$CuCl_2$]$_2$} (**1**), show the greatest activity with respect to the other compounds tested while less inhibition was show by Zn complexes. Under the reaction conditions used, the O_2^- radicals activity was almost completely inhibited by SOD at a concentration of 0.10 μM (IC50 = 0.01 μM).

The hydroxyl radical scavenging activity of the different complexes was also evaluated using the deoxyribose assay. Deoxyribose is degraded to malondialdehyde on exposure to hydroxyl radicals generated by Fenton systems. Under acidic conditions and upon heating, malondialdehyde reacts with thiobarbituric acid to form a pink chromogen which may be easily detected spectrophotometrically [45].

Table 2
SOD-like activity of different complexes.

SOD-Mimics	IC_{50} μM
(**1**){(L^1)[$CuCl_2$]$_2$}	1.82(±0.15)
(**2**){(L^1)[$Cu(OAc)_2$]$_2$}	*Not tested*
(**3**){(L^1)[$Zn(OAc)_2$]$_2$}	16.06(±0.15)
(**4**) [(CuCl(L^2)($Hpz^{Ph,Me}$)]	14.30 ((±0.40)
(**5**) [($Mn(L^3)_2(H_2O)_2$]	2.70(±0.30)
(**6**) [(Zn(OAc)(L^3)(Him)]·MeOH	17.11(±0.50)
(**7**) [(CuCl(L^4)(Him)]$_2$·(H_2O)$_2$	1.16(±0.10)

The hydroxyl radical scavenging properties were tested for all SOD-mimics using this method and no pro-oxidant effect was observed at the concentration of complexes used. The assay was performed in the absence of EDTA. As reported in Fig. 4 all compounds exhibited weak comparable scavenging activity for hydroxyl radicals except for the $\{(L^1)[Zn(OAc)_2]_2\}$ (**3**) that lacks this activity while for $[(Zn(OAc)(L^3)(Him)]\cdot MeOH$ (**6**) it is reduced with respect to the other SOD-mimics.

The superoxide scavenging activity of the complexes was also examined by EPR spin-trapping, after having established the conditions for detection of superoxide radical and interpretation of EPR spectra. After addition of XO to the reaction mixture, the EPR signal of DMPO–OOH adduct (both in the absence or presence of DMSO) was recorded at room temperature after 90 s and scans were collected thereafter for the subsequent 10 min. The characteristic spectra consisting of 12 lines with 2:4:4:2 pattern with hyperfine splitting constants $a_N = 13.89$ G, $a_H^\beta = 11.61$ G e $a_H^\gamma = 1.28$ G are reported in Fig. 1Sa,b (Supplementary material). The DMPO–OOH spectrum decays within a few minutes and is replaced by the appearance of a new signal typical of the DMPO–OH adduct (Fig. 1Sc, Supplementary material, in the absence of DMSO) characterized by a 4 line spectrum with a 1:2:2:1 pattern and hyperfine splitting constants $a_N = 14.85$ G, $a_H^\beta = 14.85$ G, or of the DMPO–CH_3 adduct (Fig. 1Sd, Supplementary material), in the presence of DMSO, characterized by a 6 line spectrum of equal intensity with hyperfine splitting constants $a_N = 16.1$ G, $a_H^\beta = 23.0$ G. Both these signals arise partly from the well known spontaneous decay of the DMPO–OOH adduct, and partly from the spontaneous dismutation of superoxide radical since this is not completely scavenged by DMPO. In the latter case, the reactions leading to the two adducts are described in Eqs. (1)–(5):

$$O_2^{\bullet -} + O_2^{\bullet -} + 2H^+ \rightarrow H_2O_2 + O_2 \quad (1)$$

$$O_2^{\bullet -} + H_2O_2 + 2H^+ \rightarrow O_2 + H_2O + OH^{\bullet} \quad (2)$$

$$DMPO + OH^{\bullet} \rightarrow DMPO{-}OH \quad (3)$$

$$OH^{\bullet} + CH_3S(O)CH_3 \rightarrow CH_3S(O)OH + CH_3^{\bullet} \quad (4)$$

$$DMPO + CH_3^{\bullet} \rightarrow DMPO{-}CH_3. \quad (5)$$

Addition of SOD (5 u/ml) to the reaction medium resulted in a loss of signal intensity due to the rapid dismutation reaction rate ($2.3\times10^9\ M^{-1}\ s^{-1}$) [51] compared with the slow trapping rate ($10\ M^{-1}\ s^{-1}$) [52].

Having established the conditions for superoxide generation and interpretation of the EPR spectra, the following metal complexes, $\{(L^1)[CuCl_2]_2\}$ (**1**), $[(CuCl(L^2)(Hpz^{Ph,Me})]$ (**4**), $[(Mn(L^3)_2]\cdot 2H_2O$ (**5**) and $[(CuCl(L^4)(Him)]_2\cdot 2H_2O$ (**7**), were tested. The other metal complexes could not be tested due to insolubility reasons at the concentrations required in this experimental system. Different concentrations for each compound were examined in order to find the concentration at which the DMPO–OOH signal at 90 s (Fig. 5a) was inhibited by roughly 50%, which corresponds to a SOD concentration of 2.5 u/ml (Fig. 5b). For compounds $[(Mn(L^3)_2]\cdot 2H_2O$ (**5**) and $[(CuCl(L^4)(Him)]_2\cdot 2H_2O$ (**7**), a 500 μM concentration lead to an appreciable decrease in the DMPO–OOH signal (Fig. 5c,d), indicating superoxide radical scavenging activity. For compound $[(CuCl(L^2)(Hpz^{Ph,Me})]$ (**4**), only a slight decrease in this signal was observed (Fig. 5e) which was unaffected by increasing its concentration. Instead complex $\{(L^1)[CuCl_2]_2\}$ (**1**) lead to roughly a 50% decrease in the DMPO–OOH signal at concentrations as low as 325 μM (Fig. 5f). However, at concentrations 400 μM and above, the DMPO–OOH signal was immediately replaced by the DMPO–CH_3 signal. This can be explained by admitting a Fenton-like activity which promotes hydroxyl radical formation and hence detection of this adduct (Eqs. (3)–(5)). In fact, Fig. 2Sa (Supplementary material) shows the DMPO–CH_3 signal obtained from 400 μM complex $\{(L^1)[CuCl_2]_2\}$ (**1**). This signal was also observed with complex $[(CuCl(L^4)(Him)]_2\cdot 2H_2O$ (**7**) but at 750 μM (Fig. 2Sb, Supplementary material). Complex $[(Mn(L^3)_2]\cdot 2H_2O$ (**5**) showed no Fenton-like activity, even at concentrations as high as 1 mM (Fig. 2Sc, Supplementary material). In this case no signal was observed because at this concentration superoxide radical is efficiently scavenged hence none is trapped by DMPO. For complex $[(CuCl(L^2)(Hpz^{Ph,Me})]$ (**4**) (Fig. 2Sd, Supplementary material), no Fenton-like activity was observed, even at 1 mM since the DMPO–OOH signal was the only signal recorded.

To further confirm that complexes $\{(L^1)[CuCl_2]_2\}$ (**1**) and $[(CuCl(L^4)(Him)]_2\cdot 2H_2O$ (**7**) were capable of generating hydroxyl radicals by Fenton-type reactions, H_2O_2 (1 mM) was added to them in the presence of DMPO and the DMPO–CH_3 signal with traces of the DMPO–OH one were immediately observed (Fig. 3Sa,b, Supplementary material). Instead, no EPR signals were observed for complexes $[(Mn(L^3)_2]\cdot 2H_2O$ (**5**) and $[(CuCl(L^2)(Hpz^{Ph,Me})]$ (**4**) (Fig. 3Sc,d, Supplementary material) as expected.

Considering that $[(Mn(L^3)_2]\cdot 2H_2O$ (**5**) is a Mn complex and since previous literature reports have demonstrated that Mn complexes are capable of scavenging hydroxyl radicals besides possessing SOD-like activity, the former activity was tested on this complex. Hydroxyl free radicals were generated by the Fenton reaction (H_2O_2/Fe^{2+}) and indirectly demonstrated by the appearance of the DMPO–CH_3 signal with traces of the DMPO–OH one (Fig. 4Sa, Supplementary material). As shown in Fig. 4Sb (Supplementary material), the presence of 1 mM of $[(Mn(L^3)_2]\cdot 2H_2O$ (**5**) lead to a remarkable decrease in intensity of this signal, a decrease which was concentration dependent (not shown). This result thus suggests the hydroxyl scavenging ability of this Mn complex which is in agreement with the results shown in Fig. 4.

Based on the results obtained by EPR-spin trapping, the potential peroxidase activity of all the complexes using a fluorescent method was investigated. As previously reported in [31], with this method it is possible to measure the peroxidase activity of SOD: incubation of the enzyme with a mixture containing DCFH and H_2O_2 causes a time dependent increase in DCF fluorescence (Fig. 6). In accordance with the EPR data, the complex $[(CuCl(L^4)(Him)]_2\cdot 2H_2O$ (7) shows the highest peroxidase activity while only a slight increase in fluorescence with respect to the control is shown for $\{(L^1)[CuCl_2]_2\}$ (1). For the other SOD-like complexes, no peroxidase activity was observed.

An important mechanism by which SOD mimics can attenuate inflammation is by reducing peroxynitrite formation by simply removing superoxide before it can react with nitric oxide. These compounds also have the possibility to react with peroxynitrite and reduce the oxidative damage it causes as reported in Fig. 7. From the

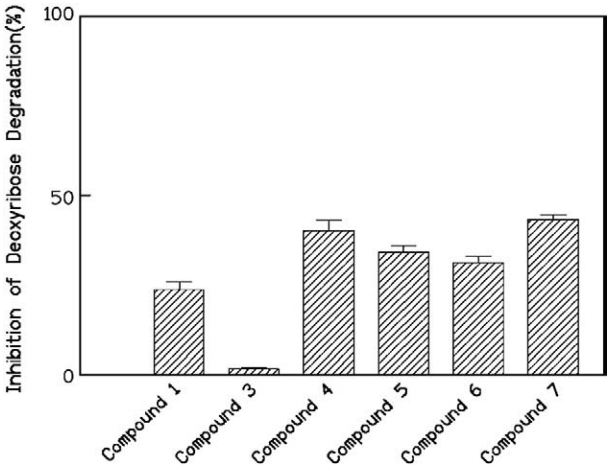

Fig. 4. Hydroxyl radical scavenging activity effects of different SOD-mimics tested at 25 μM in DMSO.

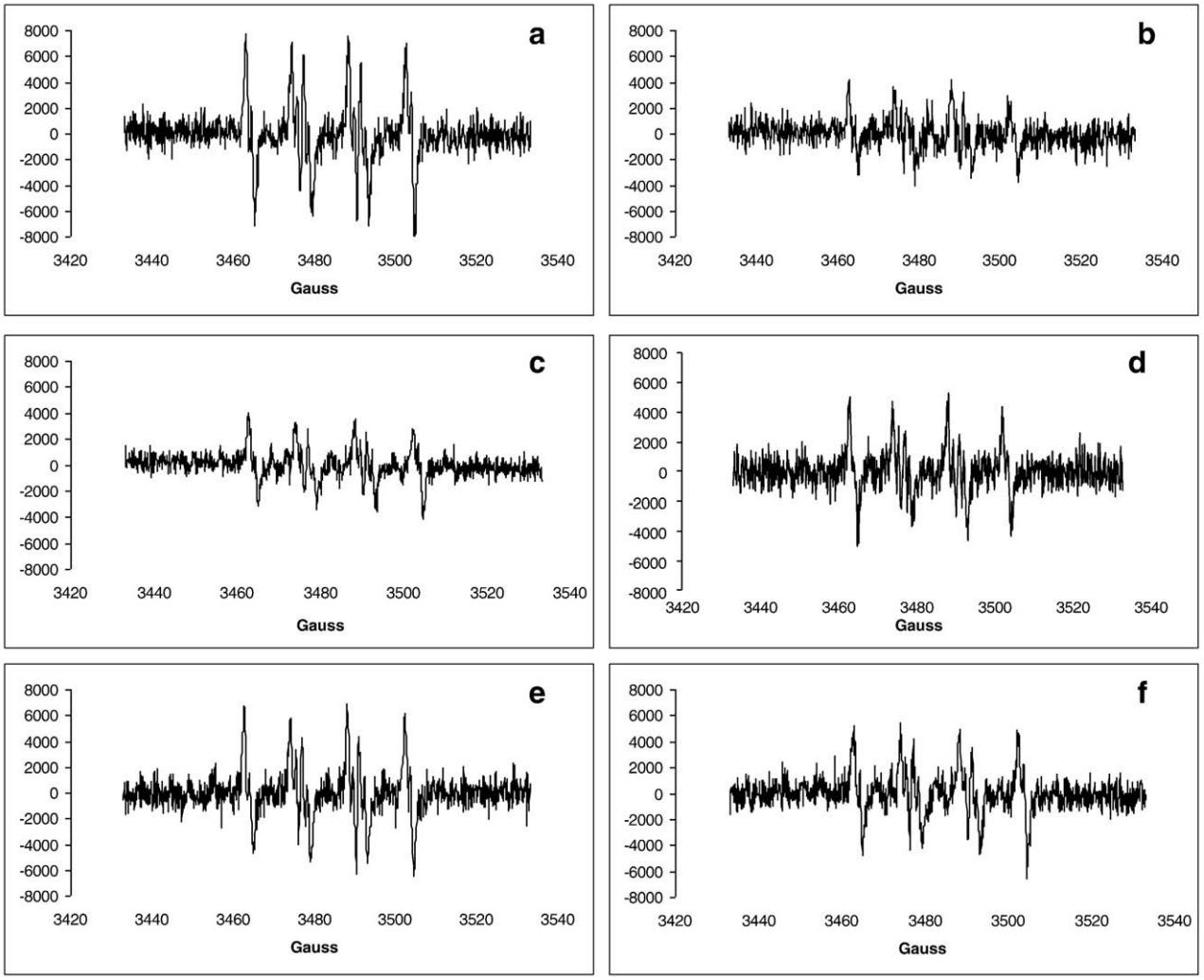

Fig. 5. EPR spin trapping of superoxide radical with DMPO in the presence of SOD-like mimics. a) DMPO–OOH obtained from HX/XO + DMSO system recorded 90 s after addition of XO; b) DMPO–OOH obtained from HX/XO + DMSO system in the presence of **SOD** 2.5 u/mL; c) DMPO–OOH obtained from a) in the presence of *[(Mn(L^3)$_2$](H$_2$O)$_2$*,(**5**) 500 μM; d) DMPO–OOH obtained from a) in the presence of *[(CuCl(L^4)(Him)]$_2$·(H$_2$O)$_2$* ,(**7**) 500 μM; and e) DMPO–OOH obtained from a) in the presence of *[(CuCl(L^2)(Hpz^{Ph,Me})]*, (**4**) 500 μM; f) DMPO–OOH obtained from a) in the presence of *{(L^1)[CuCl$_2$]$_2$}*, (**1**) 325 μM.

data obtained it is possible to note that the dinuclear metal complexes show scavenging activity against this oxidant: a remarkable reactivity was observed for [(Mn(L^3)$_2$]·2H$_2$O (**5**) with respect to the Cu and Zn derivatives (**1**), (**7**), (**3**) and (**6**) {(L^1)[CuCl$_2$]$_2$} (**1**), [(CuCl(L^4)(Him)]$_2$·2H$_2$O (**7**), {(L^1)[Zn(OAc)$_2$]$_2$} (**3**), [(Zn(OAc)(L^3)(Him)]·MeOH (**6**) (that show comparable activity) whereas this is totally absent in the [(CuCl(L^2)(Hpz^{Ph,Me})] (**4**) derivative. In particular, the activity of the Mn complex was further investigated and as reported in the inset of Fig. 7, its scavenging activity is concentration-dependent.

4. Discussion

Recent advances in medicinal inorganic chemistry demonstrate significant perspectives for the utilization of metal complexes as drugs, presenting a flourishing area of work for inorganic chemistry [7–10]. In this study, different Cu, Zn and Mn dinuclear complexes with some neutral and monoanionic pyrazole-based ligands were synthesized and characterized and their radical scavenging properties evaluated. Some of these compounds are not soluble in solvents that can be used for biological purposes hence it was impossible to evaluate their potential activities. All DMSO-soluble tested complexes, catalyze superoxide dismutation with an IC$_{50}$ in the micromolar range (Table 2). Even if in strong polar solvents such as DMSO a certain degree of ionization of our

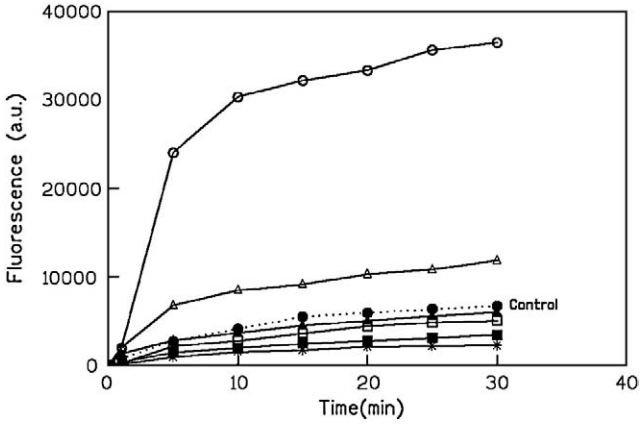

Fig. 6. Evaluation of peroxidase activity of different SOD-mimics. Time-dependent fluorescence measurement of DCF formation (excitation λ = 495 nm; emission λ = 520 nm) was performed on incubation mixtures containing DCFH (2.5 mM), H$_2$O$_2$ (1 mM), phosphate buffer 0.1 M, pH 7.4 (containing DTPA (100 μM)) and (●) DCFH alone; (○)*[(CuCl(L^4)(Him)]$_2$·(H$_2$O)$_2$*, (**7**); (Δ)*{(L^1)[CuCl$_2$]$_2$}*(**1**); (▲) *[(CuCl(L^2)(Hpz^{Ph,Me})]*(**4**); (□)*[(Zn(OAc)(L^3)(Him)]·MeOH*,(**6**); (■) *[(Mn(L^3)$_2$](H$_2$O)$_2$*,(**5**); (*){(L^1)[Zn(OAc)$_2$]$_2$} (**3**). The concentration for all compounds tested was 25 μM.

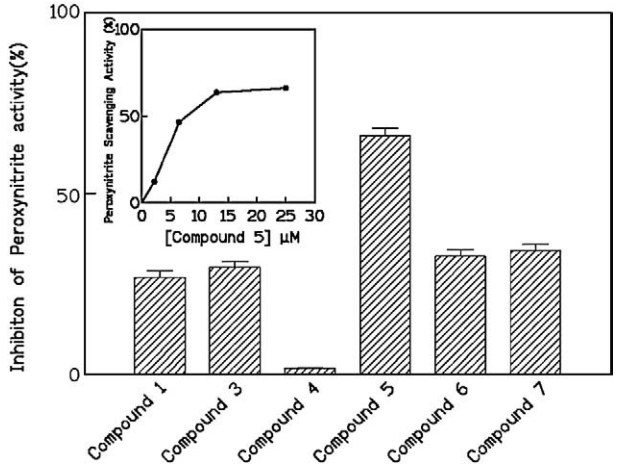

Fig. 7. Evaluation of peroxynitrite scavenging activity of different SOD-mimics. Inhibition of peroxynitrite-mediated dichlorodihydrofluorescein oxidation by different SOD mimics (25 μM) detected by fluorescence measurements. Data are expressed as the mean ± SD for three replicate determinations. Experimental condition as reported in methods. Inset: peroxynitrite scavenging activity as a function of different *[(Mn(L^3)$_2$](H$_2$O)$_2$*,(***5***) concentrations. The fluorescence measurement of DCF formation was obtained after a 15-min incubation of mixtures (as described in Materials and methods) at 25 °C, containing different concentrations of complex.

derivatives cannot be excluded, the remarkable SOD activity observed for Cu-complexes ([(CuCl(L^4)(Him)]$_2$·2H$_2$O (**7**) and {(L^1)[CuCl$_2$]$_2$} (**1**)) is probably related to the resemblance of their coordination environments with that in the native SOD enzyme. Increasing the steric hindrance in the Cu coordination environment as in derivative [(CuCl(L^2)(Hpz^{Ph,Me})] (**4**) does not increase the activity of the mimics. The synthesis of dinuclear Zn mimics lead to two derivatives with decreasing SOD-like activity that are however indicative for constructing new promising Cu–Zn stable complexes. For these derivatives it is important to determine whether a compound is in fact acting as a true catalytic SOD mimic and to this end, the activity of the complexes using EPR spectroscopy was evaluated which confirms the data obtained with indirect methods. From the results of the above EPR experiments, it may be concluded that with the exception of [(CuCl(L^2)(Hpz^{Ph,Me})] (**4**) which showed negligible SOD-like activity, at least under the experimental conditions used in this study, all the other complexes were capable of dismutating superoxide radical, {(L^1)[CuCl$_2$]$_2$} (**1**) being the most active, i.e. 50% reduction in DMPO–OOH signal at concentrations <350 mM. However, besides this superoxide scavenging activity, both {(L^1)[CuCl$_2$]$_2$} (**1**) and especially [(CuCl(L^4)(Him)]$_2$·2H$_2$O (**7**) also generate hydroxyl radicals when used at high concentrations. This result is not surprising since these two complexes both contain Cu as the active metal for SOD mimic activity, which has the potential to participate in Fenton chemistry. Therefore, the only complex which appears to have superior antioxidant properties compared to the others tested, is the Mn complex [(Mn(L^3)$_2$]·2H$_2$O (**5**) which not only scavenges superoxide radical, but also the toxic hydroxyl radical (Fig. 4). An important consideration on the catalytic activity of the different compounds as SOD-mimics is that they can act as oxidoreductases in vitro and in vivo assays. As oxidoreductases, SOD-mimics may react with superoxide in a reduction reaction but they can also react with the product of dismutation, H_2O_2 hence it is possible that an apparent catalytic redox cycle may possibly occur. This behaviour is not new because even Cu–Zn–SOD enzymes show this property, which is however absent in the mitochondria Mn–SOD form of the enzyme [53]. The pro-oxidant properties of different SOD-like mimics were evaluated using EPR and fluorescence methods and as reported in the Results section, the dinuclear copper complexes [(CuCl(L^4)(Him)]$_2$·2H$_2$O (**7**) and {(L^1)[CuCl$_2$]$_2$} (**1**) show this activity under our experimental conditions, while it is absent in the case of Mn, and Zn complexes [(Mn(L^3)$_2$]·2H$_2$O (**5**) and *[(Zn(OAc)(L^3)(Him)]·MeOH* (**6**). As an important non-enzymatic antioxidant, Zn complexes are attracting ample attention from researchers [54] and it can be seen that the inhibitory effects of the zinc derivatives *{(L^1)[Zn(OAc)$_2$]$_2$}* (**3**) and *[(Zn(OAc)(L^3)(Him)]·MeOH* (**6**) against $O_2^{-\cdot}$ and ·OH radicals are related to concentration. Our results are in line with those reported in different studies where it has been demonstrated that different zinc salts [55] or zinc complexes prepared with pharmacologically active ligands [56–58] possess potent antioxidant activity, and can attenuate the biochemical consequences of oxygen free radicals. In particular, Zn-complexes seem to be active scavengers of OH·.

The pro-oxidant activity of the two Cu complexes is totally reduced in the concentration range around the IC_{50} values (data not shown). In view of the critical role of the superoxide radical in several disease states, these new dinuclear SOD-like mimics also appear to react with relevant biological oxidants, in particular with peroxynitrite. This is important since the pro-inflammatory and cytotoxic effects of peroxynitrite in tissues are numerous and the removal of peroxynitrite by agents such as SOD-like mimics may be cytoprotective and anti-inflammatory [59,60]. From the data reported in Fig. 7, the complexes may be ranked according to their scavenging activity towards peroxynitrite. The complex [(Mn(L^3)$_2$]·2H$_2$O (**5**) shows the highest reactivity which is twice that of the Cu and Zn derivatives. Therefore from this preliminary screening on the scavenging properties of these new dinuclear complexes, the only compound which appears to have superior antioxidant properties compared to the others tested is the complex [(Mn(L^3)$_2$]·2H$_2$O (**5**) which besides scavenging superoxide radical, does not show any prooxidant activity at high concentrations. The dinuclear Mn compounds could be considered good candidates for use as human pharmaceuticals as previously reported for other mononuclear Mn complexes [6] for which biological and kinetic data are available. Several biological studies have been published for Mn(III)(salen) complexes, Mn(III)(porphyrinato) complexes, Mn(II)(1,4,7,10,13-pentaazayclopentadecane) and Mn(II) bis(cyclohexylpyridine)-substituted (M40403) derivatives (for review see Refs. [6,10,12,61]), which have been shown to be promising active drugs in clinical therapy for diseases mediated by superoxide radicals. The IC_{50} value exhibited by [(Mn(L^3)$_2$]·2H$_2$O (**5**) is lower than those reported for other Cu–SOD mimics, nevertheless, further investigations should be done regarding with the stability of the metals in their complexes, their toxicity and importantly, their biological effects at the cellular level. These studies are in progress in our laboratory and currently we continue to investigate new strategies to enhance the ROS-scavenging systems of the cell, in an effort to attenuate the damage resulting from oxidative stress. SOD is in fact one of the first line ROS-defence enzymes in cells whose role is becoming increasingly important as more pathological and disease states are discovered to be linked with oxidative damage.

Table of abbreviations

L^1	1-(2-(4-((2,2,2-tris(pyrazol-1-yl)ethoxy)methyl)benzyloxy)-1,1-di(pyrazol-1-yl)ethyl)-pyrazole
K[L^2]	potassium hydridotris(3-phenyl-5-methylpyrazolyl)borate
HL^3	bis(pyrazol-1-yl)acetic acid
HL^4	bis(3,5-dimethylpyrazol-1-yl)acetic acid
OAc	acetate
Hpz^{Ph,Me}	3-phenyl-5-methylpyrazole
imH	imidazole
THF	tetrahydrofuran
EPR	electron paramagnetic resonance
IC_{50}	inhibiting concentration of 50% target substrate
ROS	reactive oxygen species
SOD	superoxide dismutases
HX	hypoxanthine
XO	xanthine oxidase

CAT	catalase
PMS	phenazine methosulfate
NBT	nitroblue-di tetrazolium chloride
DMPO	5,5-dimethyl-1-pyrroline-N-oxide
DTPA	Diethylene triamine pentaacetic acid
DCFH	2,7-dichloro-fluorescin

Acknowledgements

Financial supports by the University of Camerino, Fondazione CARIMA and Valle-esina Spa are gratefully acknowledged. Authors are also grateful to the Italian Ministry of University and Research – International University cooperation programs-2009 – for the financial support.

Appendix A. Supplementary data

Supplementary data associated with this article can be found, in the online version, at doi:10.1016/j.jinorgbio.2010.03.013.

References

[1] A.D. de Grey, Free Radic. Res. 40 (2006) 1244–1249.
[2] F. Johnson, C. Giulivi, Mol. Aspects. Med. 26 (2005) 340–352.
[3] J.R.J. Sorenson, Curr. Med. Chem. 9 (2002) 639–662.
[4] D. Salvemini, Z.-Q. Wang, J.L. Zweier, A. Samouilov, H. Macarthur, T.P. Misko, M.G. Currie, S. Cuzzocrea, J.A. Sikorski, D.P. Riley, Science 286 (1999) 304–306.
[5] C.X. Zhang, S.J. Lippard, Curr. Op. Chem. Biol. 7 (2003) 481–489.
[6] D.P. Riley, Chem. Rev. 99 (1999) 2573–2588.
[7] H. Sakurai, Y. Kojlwe, Y. Yoshikawa, K. Kewebe, H. Yosul, Coord. Chem. Rev. 226 (2002) 167–178.
[8] B.J. Day, Antioxid. Redox Signal 10 (2008) 355–370.
[9] V. Afonso, R. Champy, D. Mitrovic, P. Collin, A. Lomri, Joint Bone Spine. 74 (2007) 324–329.
[10] A.S. Potapov, E.A. Nudnova, G.A. Domina, L.N. Kirpotina, M.T. Quinn, A.I. Khlebnikov, I.A. Schepetkin, Dalton Trans. 23 (2009) 4488–4498.
[11] M. Cejuedo, S. Alzuet, S. Ferrer, J. Borra, A. Castineiras, A. Mozzani, L. Casella, Inorg. Chem. 43 (2004) 6805–6814.
[12] V.S. Sprakel, M.C. Feiters, W. Meyer-Klaucke, M. Klopstra, J. Brinksma, B.L. Feringa, K.D. Karlin, R.J. Nolte, Dalton Trans (2005) 3522–3527.
[13] S. Tabassum, S. Parveen, F. Arjmand, Indian J. Chem. 43A (2004) 270–277.
[14] S. Tabassum, S. Parveen, F. Arjmand, Trans. Met. Chem. 30 (2005) 196–204.
[15] F. Arjmand, S. Parveen, S. Tabassum, Trans. Met. Chem. 30 (2005) 128–135.
[16] I. Schepetkin, A. Potapov, A. Klebnikov, E. Korotkova, A. Lukina, G. Malovichko, L. Kirpotina, M.T. Quinn, J. Biol. Inorg. Chem. 11 (2006) 499–513.
[17] P. Chen, K. Fujisawa, E.I. Solomon, J. Am. Chem. Soc. 122 (2000) 10177–10193.
[18] G. Parkin, Chem. Rev. 104 (2004) 699–768.
[19] U.P. Singh, A.K. Sharma, P. Tyagi, S. Upreti, R.K. Singh, Polyhedron 25 (2006) 3628–3638.
[20] A.D. Schofield, M.L. Barros, M.G. Cushion, A.D. Schwarz, P. Mountford, Dalton Trans. (2009) 85–96.
[21] A. Beck, B. Weibert, N. Burzlaff, Eur. J. Inorg. Chem. (2001) 521–527.
[22] I. Hegelmann, A. Beck, C. Eichhorn, B. Weibert, N. Burzlaff, Eur. J. Inorg. Chem. (2003) 339–347.
[23] B.S. Hammes, M.T. Kieber-Emmons, J.A. Letizia, Z. Shirin, C.J. Carrano, L.N. Zakharov, A.L. Rheingold, Inorg. Chim. Acta 346 (2002) 227–238.
[24] B. Kozlevčar, P. Gamez, R. de Gelder, W.L. Driessen, J. Reedijk, Eur. J. Inorg. Chem. (2003) 47–50.
[25] G.A. Santillan, C.J. Carrano, Inorg. Chem. 46 (2007) 1751–1759.
[26] G.A. Santillan, C.J. Carrano, Dalton Trans (2008) 3995–4005.
[27] G.A. Santillan, C.J. Carrano, Inorg. Chem. 47 (2008) 930–939.
[28] B. Kozlevčar, A. Golobič, P. Gamez, I.A. Koval, W.L. Driessen, J. Reedijk, Inorg. Chim. Acta 358 (2005) 1135–1140.
[29] M. Pellei, G. Gioia Lobbia, C. Santini, R. Spagna, M. Camalli, D. Fedeli, G. Falcioni, Dalton Trans (2004) 2822–2828.
[30] L. Peters, E. Hübner, T. Haas, F.W. Heinemann, N. Burzlaff, J. Organomet.Chem 694 (2009) 2319–2327.
[31] E. Hübner, T. Haas, N. Burzlaff, Eur. J. Inorg. Chem. (2006) 4989–4997.
[32] N. Burzlaff, I. Hegelmann, B. Weibert, J. Organomet. Chem. 626 (2001) 16–23.
[33] N. Burzlaff, in: R. van Eldik (Ed.), Tripodal N,N,O-Ligands For Metalloenzyme Models And Organometallics, Adv. Inorg. Chem., Vol. 60, Elsevier, London, 2008, pp. 101–165.
[34] A. Otero, J. Fernández-Baeza, A. Lara-Sánchez, J. Tejeda, L. F: Sánchez-Barba, Eur. J. Inorg. Chem (2008) 5309–5326.
[35] R.M. Uppu, G.L. Squadrito, R. Cueto, W.A. Pryor, Methods Enzymol. 269 (1996) 311–312.
[36] M.W. Senko, IsoPro Isotopic Abundance Simulator, v. 2.1, National High Magnetic Field Laboratory, Los Alamos National Laboratory, Los Alamos, NM, 1994.
[37] D.L. Reger, T.D. Wright, R.F. Semeniuc, T.C. Grattan, M.D. Smith, Inorg. Chem. 40 (2001) 6212–6219.
[38] K.-W. Yang, Y.-Z. Wang, Z.-X. Huang, J. Sun, Polyhedron 16 (1997) 109.
[39] F. Marchetti, M. Pellei, C. Pettinari, R. Pettinari, E. Rivarola, C. Santini, B.W. Skelton, A.H. White, J. Organomet. Chem. 690 (2005) 1878–1888.
[40] H. Kopf, C. Pietraszuk, E. Hübner, N. Burzlaff, Organometallics 25 (2006) 2533–2546.
[41] G.M. Sheldrick, SHELXL-97: Crystal Structure Refinement Program, University of Göttingen, Germany, 1997.
[42] Version 3.0, Bruker AXS, 2005, Karlsruhe, Germany.
[43] D.L. Reger, R.F. Semeniuc, C. Pettinari, F. Luna-Giles, M.D. Smith, The cartesian coordinates of the ligand L^1 were derived from the experimentally determined crystal structure of a ruthenium dimer, Crystal Growth Des. 6 (2006) 1068–1070.
[44] P. Valentão, E. Fernes, F. Carvalho, P.B. Andrade, R.M. Seabra, M.L. Bastos, J. Agric, Food Chem. 49 (2001) 3476–3479.
[45] M. Paya, B. Halliwell, J.R.S. Hoult, Biochem. Pharmacol. 44 (1992) 205–214.
[46] H. Zhang, J.M. Gurney, D. Becker, B. Kalyanaraman, J. Biol. Chem. 277 (2002) 1013–1020.
[47] W.J. Geary, Coord. Chem. Rev. 7 (1971) 81–122.
[48] K. Nakamoto, Infrared and Raman Spectra of Inorganic and Coordination Compounds, 6th Ed., Part B, John Wiley & Sons, Hoboken, New Jersey, 2009, pp. 62–67, and references reported therein.
[49] C. Pettinari, Scorpionates II: Chelating Borate Ligands, Imperial College Press, London, 2008.
[50] C. Pettinari, F. Marchetti, R. Pettinari, A. Marinelli, A. Crispini, A. Bellusci, Inorg. Chim. Acta 362 (2009) 4593–4598.
[51] E. Finkelstein, G.M. Rosen, E.J. Raukman, J. Am. Chem. Soc 102 (1980) 4994–4999.
[52] E.M. Fielden, P.B. Roberts, B.C. Bray, D.J. Lowe, G.N. Mautner, G. Rotilio, L. Calabrese, Biochem. J. 139 (1974) 49–60.
[53] T. Offer, A. Russo, A. Samuni, FASEB J. 14 (2000) 1215–1223.
[54] A. Formigari, P. Irato, A. Santon, Comp. Biochem. Physiol., Part C 146 (2007) 443–459.
[55] D. Bagchi, M. Bagchi, S.J. Stohs, Gen. Pharmac. 28 (1997) 85–91.
[56] Q. Wang, Y. Wang, Z. Yang, Chem. Pharm. Bull. 56 (2008) 1018–1021.
[57] T.R. Li, Z.Y. Yang, B.D. Wang, Chem. Pharm. Bull. 55 (2007) 26–32.
[58] D. Qin, Z. Yang, G. Qi, Spectrochim. Acta A 74 (2009) 415–420.
[59] C. Muscoli, S. Cuzzocrea, D.P. Riley, J.L. Zweier, C. Thiemermann, Z.Q. Wang, D. Salvemini, Br. J. Pharmacol. 140 (2003) 445.
[60] E. Esposito, S. Cuzzocrea, Front. Biosci. 14 (2009) 263.
[61] Y. Xu, B. Liu, J.L. Zweie, G. He, J. Pharmacol. Exp. Ther. 327 (2008) 402.